Determining finite strain: how far have we progressed?

Dave McCarthy[1], Patrick Meere[2] and Kieran Mulchrone[3]

1 British Geological Survey, The Lyell Centre, Research Avenue South, Edinburgh, EH14 4AP, UK

2 School of Biological, Earth and Environmental Sciences, University College, Cork, Ireland

3 Department of Applied Mathematics, University College, Cork, Ireland

Abstract

One of the main aims in the field of structural geology is the identification and quantification of deformation or strain. This pursuit has occupied geologists since the 1800's, but has evolved dramatically since those early studies. The quantification of strain in sedimentary lithologies was initially restricted to lithologies of known initial shape, such as fossils or reduction spots. In 1967, Ramsay presented a series of methods and calculations, which allowed populations of clasts to be used as strain markers. These methods acted as a foundation for modern strain analysis, and have influenced thousands of studies. This review highlights the significance of Ramsay's contribution to modern strain analysis. We outline the advances in the field over the 50 years since publication of the 'Folding and Fracturing of Rocks', review the existing limitations of strain analysis methods and look to future developments.

'The analysis of the variation in amount of finite strain in a deformed zone is of the utmost importance in helping to understand the structural geometry and hence the structural history of the rocks.'

John Ramsay, 1967

The field of structural geology is primarily concerned with understanding the deformation of crustal rocks. This deformation or strain is caused when external forces or stresses act on a rock mass, causing a change in its shape or size (Ramsay, 1967). The concept of quantifying strain in rocks has been prevalent since the 1800's, and has evolved dramatically since those early studies. Various methods have been used to identify and quantify strain, the earliest of which relied on objects of a known initial

shape. This approach was first taken by Phillips (1843) and Sharpe (1847) who used deformed fossils, with Sharpe (1847) noting that the most deformed fossils were present in the areas with the most intense cleavage. This led to Sorby's seminal interpretations of cleavage development (Sorby, 1849) and correlation of cleavage to areas with high strain (Sorby, 1856). Haughton (1856) provided the first mathematical description of length changes in fossils due to strain in naturally deformed rocks, furthermore, he applied the concept of the strain ellipsoid to rock deformation, which established a framework for strain to be quantified and compared.

It was not until the quantitative studies on distorted ooids by Cloos (1947) that truly numerical and methodological strategies were fully applied to strain analysis. By the early 1960's, strain analysis methods were still largely dependent on the presence of strain markers of known initial shape, such as fossils, ooids or reduction spots (Breddin, 1954, 1957; DeSitter, 1964). In 1967, John Ramsay presented a suite of precise and mathematical procedures that allowed for the accurate determination of finite strain in deformed rocks. These methods, though significantly modified, have stood the test of time and are regularly employed. Of the many publications citing Ramsay's Folding and Fracturing, a significant number, >1000, have focussed on strain analysis (Lisle, this issue). It is clear that these techniques are still applied to both field studies and mathematical models of rock deformation.

This review starts by highlighting the importance of Ramsay's initial contribution, then we outline the significant advances in the techniques of strain analysis made over the last 50 years. This is followed with a brief discussion on applications of strain analysis and how these techniques have advanced our understanding of natural rock deformation. There is clearly a huge body of research involving strain analysis and it is not possible to reference every application here, but we have highlighted some key developments. We then follow this by providing a discussion of some of the key unresolved problems in the field. We conclude with some ideas for future directions and hope that this will act as a springboard for those investigating strain in rocks for the first time.

Strain Analysis Techniques proposed by Ramsay

The significance of Ramsay's contribution was that he set out in a systematic and mathematical manner techniques for determining strain from objects of known initial shape, and he established methods which allowed populations of objects, such as sedimentary clasts, of non-spherical and fluctuating initial shape, to be used as strain markers. These methods depend on clast orientation, repacking and intraclast deformation of clasts due to deformation. This was a key development in strain analysis, as it allowed estimates to be made from lithologies that did not have obvious or established strain markers (Fig. 1). The methods developed by Ramsay (1967) are briefly outlined below:

Method 1

The first method that Ramsay outlined built on existing techniques at the time, and involved direct measurement of the principal axes of elliptical strain markers and the orientation of their long axes (Ramsay, 1967, p 193). These axes are then plotted against each other (Fig. 2a) and the slope of the best-fit line that also passes through the origin provides an estimate of the strain ratio (Fig. 2b). Ramsay noted it was difficult to accurately identify ellipse lengths in high deformation regimes, and that it was difficult to identify the maximum stretching direction in low strain regimes.

Method 2

The second method (Ramsay, 1967, p 193-194), does not rely on direct measurement of ellipse axes, and accounts for difficulties in methods of identifying the length of maximum ellipse axes. The centre of each ellipse is identified and the lengths of chords from the centre to the edge of each ellipse along three arbitrarily directions are measured. The sum of the chord lengths for the three defined directions for a population of objects is calculated (Fig. 2c). If the objects were initially circular, the ratios of elongation can be calculated for each direction.

Method 3

This method, commonly referred to as the nearest-neighbour or centre-to-centre method, (Ramsay, 1967, p 195-196) was developed to tackle cases where pressure solution was suspected to have occurred, and is applicable to rocks with particles equally or unequally distributed throughout the rock mass. In cases where pressure solution is a significant deformation mechanism, the elliptical shape or preferred orientation of markers is not reliable. This method is particularly useful for identifying cases where non-passive deformation is thought to have occurred (i.e. that the clasts are not deforming homogeneously with the matrix). The basic premise involves measuring the distance between object centres, and assuming that in the unstrained state these distances should be isotropic (Fig. 3a). During deformation the distance between centres should become shorter parallel to the maximum compression axis (Fig. 3b & c).

Method 4

The fourth method (Ramsay, 1967, p 197-199) utilised the measurements of distorted angles of radial and tangential lines in elliptical sections, such as those in spherulites. Whilst an elegant method of calculating strain, this method has had limited use due to the specific nature of the strain markers required.

$R_f/\emptyset$ *Method*

In addition to the four methods above, Ramsay (1967, p 204-211) also outlined a method for specifically dealing with markers of initial elliptical, the $R_f/\emptyset$ method (Fig. 4), where R_f is the deformed axial ratio of the marker ellipsoid, while $\emptyset$ is the orientation of the long axis. This is slightly more complex than using initially circular objects, in that when an ellipse is deformed under homogeneous conditions, the resulting shape is another ellipse. The axial ratio (R_f) and orientation of the deformed ellipse is a result of the combination of the initial aspect ratio (R_i) and orientation (θ), and the strain

ellipse, all of which are unknowns. When a population of deformed ellipses are considered, variations in their Ø values can be related to eccentricity in their orientations prior to deformation.

Measuring strain after Ramsay

Essentially Ramsay (1967) developed methods whereby strain estimates could be made using parameters derived from the following: strain marker orientation, strain marker shape, position of strain marker centres, distance between centres and the angle between centres. The two main types of methods that prevailed were the $R_f/Ø$ method and the centre-to-centre. The $R_f/Ø$ method (Fig. 4) determines finite strain from randomly oriented populations of deformed elliptical objects, while the centre-to-centre method (Fig. 3) uses the distance between centres of adjacent objects, and assumes the objects were uniformally distributed prior to deformation.

Subsequent to the initial $R_f/Ø$ method, alternative methods based on marker shape and orientation were developed (Dunnet, 1969; Elliott, 1970; Dunnet and Siddans, 1971; Matthews et al., 1974; Borradaile, 1976; Shimamoto and Ikeda, 1976; Lisle, 1977a, 1977b, 1985; Robin, 1977; Peach and Lisle, 1979; Siddans, 1980; Yu and Zheng, 1984; Mulchrone and Meere, 2001; Mulchrone et al., 2003). Dunnet (1969) developed an $R_f/Ø$ diagram method, while Elliott (1970) applied a similar graphical approach, the shape factor grid. Dunnet and Siddans (1971) took non-random initial orientations into consideration for the $R_f/Ø$ diagram method. A significant drawback of these methods is that they are subjective.

An algebraic method that accommodated statistical analysis of any errors produced was introduced by Matthews et al. (1974). The drawback of this method was that the orientation of the principal strain axis needed to be calculated independently prior to using the method. Similarly, Robin (1977) derived a method that allowed analysis of strain markers of any shape but required prior independent knowledge of the principal strain axes. Advances in the $R_f/Ø$ method are discussed in further detail by Lisle (1994). In order to address the issues outlined above with calculating strain from distributions of elliptical objects, Shimamoto and Ikeda (1976) developed an objective non-graphical, reproducible

123 approach to strain analysis. This approach averaged the parameters of all of the marker ellipses to
124 generate one marker ellipse, or if the initial distribution was isotropic, a marker circle. The Mean Radial
125 Length (MRL) method of Mulchrone et al. (2003) took a similar approach, whereby the average shape
126 of a population of isotropic ellipses or non-deformed sedimentary clasts equates to a circle. As this
127 population becomes deformed by either shape change or rotation, this circle becomes an ellipse
128 and can be directly related to the strain ellipse in the same manner that any circular marker can
129 after deformation.

130 The centre-to-centre family of techniques are based on using object-to-object separation and assume
131 that the distribution of marker objects are isotropic and that after deformation the distance between
132 any marker centre and all other clast centres has been modified. The relative change in clast centres
133 distances can be related to the direction and magnitude of the finite strain ellipse (Ramsay, 1967).
134 Compared to the Rf/Ø method, the centre-to-centre method involved relatively complicated
135 calculations and was particularly labour intensive. As a result, it initially received significantly less
136 attention than the Rf/Ø method. This changed when a relatively simple graphical approach was
137 developed by Fry (1979; Hanna and Fry, 1979), which used all object-object separations. This was
138 subsequently further improved as the Normalised Fry Method (Erslev, 1988) and the enhanced
139 Normalised Fry Method (Erslev and Ge, 1990). McNaught (1994) further extended these methods by
140 facilitating the use of non-elliptical markers by determining best-fit ellipses for these irregular shaped
141 objects. One of the drawbacks of the centre-to-centre techniques is that they do not account for
142 volume loss, which can be considerable when pressure solution is a dominant deformation mechanism
143 (Onasch, 1986; Dunne et al., 1990). Furthermore, if pressure solution is significant, there are
144 difficulties in identifying the pre-strain centres of clasts and if significant heterogeneous deformation
145 is present at the clast scale than this can lead to further underestimates of strain.

146 The Fry methods have been regularly incorporated into automated analysis tools (Ailleres et al., 1995;
147 Launeau and Robin, 1996; Launeau et al., 2010). Despite popularity and ease of use, these methods

148 are subjective, with interpreter bias being introduced at both the identification of clast centres, and
149 the definition of the central ellipse on the Fry plot. Mulchrone (2003) used Delaunay triangulation to
150 characterise nearest neighbour separations, and defined object centres using the centroid of the best-
151 fit ellipse. This resulted in a more objective and automated process for identifying object centres and
152 creating the tie-lines between nearest neighbours.

153 *Calculating the strain ellipsoid*

154 Most strain analysis techniques focus on quantifying strain in a 2D plane. In order to quantify strain in
155 3D, a strain ellipsoid needs to be defined. Typically, the strain ellipsoid is defined from strain ellipses
156 on several planar surfaces with differing orientations. Similar to calculating the strain ellipse,
157 calculating the strain ellipsoid is not a trivial process, and numerous attempts have been made at
158 determining the most accurate best-fit ellipsoid. Ramsay (1967; p. 142-147) derived a series of
159 equations to solve for the best-fit ellipsoid from three mutually perpendicular planes. Numerical
160 algorithms were subsequently developed for three orthogonal sections (Shimamoto and Ikeda, 1976;
161 Oertel, 1978). This was followed by methods, which allowed for non-orthogonal sections (Milton,
162 1980; Gendzwill and Stauffer, 1981; Shao and Wang, 1984; De Paor; 1990). Owens (1984) in particular
163 described an iterative method for the calculation of the best-fit strain ellipsoid from any number of
164 non-perpendicular sections using a least squares approach, as well as applying a scale factor. Robin
165 introduced an approach utilising a series of linear equations (Robin, 2002; Launeau and Robin, 2005).
166 Shan (2008) built on the Robin method, and included added flexibility, whereby stretching lineation
167 data could be included. The important distinction of the Robin and Shan methods from the previous
168 methods was that they were non-iterative but separated the parameters to be calculated from the
169 initial data. Vollmer (2017) has provided a more detailed comparison of the Robin and Shan methods,
170 as well as applying bootstrap statistics to the results. Mookerjee and Nickleach (2011) presented a
171 suite of methods in Mathematica, which attempts to minimise the errors between the best-fit ellipsoid
172 and any of the measured planes used as input data.

Graphical representation of the strain ellipsoid

The geometries of strain ellipsoids can be represented in 2D space using a Flinn Plot (Flinn, 1956, 1962, 1965). This type of plot was first used to compare the elliptical properties of clast populations in conglomerates (Zingg, 1935). The ratio of the maximum to intermediate ellipsoid axes (R X/Y) is plotted as ordinate and the ratio of the minimum to intermediate axes (R Y/Z) is plotted as abscissa on these graphs. The Flinn Plot was subsequently modified by Ramsay (1967) to include a logarithmic scale (Fig. 5; discussed further in Hobbs et al., 1976; Ramsay and Huber, 1983). The benefit of the logarithmic Flinn Plot is that it provides a more even distribution of points with increase in deformation (Ramsay and Huber, 1983), whilst in the original Flinn Plot low strains are clustered near the origin, making it difficult to interpret data.

The symmetry of the strain ellipsoid can be described by the ratio K ((X/Y)/(Y/Z)). If K>1 then the ellipsoid is considered to have a prolate or axial symmetric constriction and has one long axis and two shorter axes. If K<1 the ellipsoid is considered to be oblate or axially symmetrically flattened and has two long axes and one shorter axis. Between these two fields of flattening and constriction is the field of plane strain (K=1) and which only occurs when strain is acting in the XZ plane. K represents the slope of a line from the data point to the origin at (1,1), so that K=a-1/b-1 with a=x/y and b=y/z. K on the diagram can define a series of domains, so that when K=0 the finite strain ellipsoid is uniaxial oblate and has been flattened perpendicular to Z. As K tends towards 1 the ellipsoid moves away from being purely uniaxial, but remains in the oblate and flattened domain. For K values greater than 1 the ellipsoid lies in the prolate or constrictive domain, and for K=∞ the ellipsoid is purely uniaxial prolate and stretched along the X axis (Park, 1997). The degree of how far removed the ellipsoid is from spherical (ellipsoid eccentricity) is calculated as √((X/Y)2 + (Y/Z)2).

A less-popular alternative to the Flinn Plot, the Nadai-Hsu Plot (Fig. 5; Nadai, 1950; Hsu, 1966) was first applied to geological strain analysis by Hossack (1968). This type of plot presents strain in a polar area, and is argued to provide a less distorted representation of the deviatoric strains (Hobbs et al.,

198 1976; Brandon, 1995; Mookerjee and Peek, 2014). Another advantage of this type of polar plot is that
199 ellipsoids with low strain ratios plot closer together regardless of the ellipsoid shape. Ramsay and
200 Huber (1983) criticised the Nadai-Hsu plots, irrotational strain is assumed, while most natural
201 deformation involves progressive non-coaxial rotational strains.

202 The fundamental difference is that the Nadai-Hsu Plots use the *amount of strain* (εs) and Lode's Ratio
203 (ν), to define the ellipsoid shape (Lode, 1926). The *amount of strain*, is related to the octahedral shear,
204 Υo, and is defined by: $\varepsilon s = (\sqrt{3} / 2)\, \Upsilon o$, where $\Upsilon o = (2/3)\, [(\varepsilon 1 - \varepsilon 2)^2 + (\varepsilon 2 - \varepsilon 3)^2 + (\varepsilon 3 - \varepsilon 1)^2]^{½}$ and ε1,
205 ε2 and ε3 represent the strain axes. The Lode Ratio is defined as $\nu = (2\varepsilon 2 - \varepsilon 1 - \varepsilon 3) / (\varepsilon 1 - \varepsilon 3)$ and
206 ranges from -1 to 1. Lode ratios of -1 define a prolate ellipsoid, while 1 and 0, define an oblate and
207 plane strain ellipsoid respectively. Whereas the Flinn Plot solely relies on the aspect ratios of the strain
208 ellipsoid (as discussed above). For a more in depth discussion of the merits of each method readers
209 are referred to Mookerjee and Peek (2014) and Vollmer (2017).

210 *Automation*

211 Possibly one of the biggest drawbacks to most strain analysis studies is the high labour intensity
212 required for both the identification of object boundaries, and the accurate identification of their
213 centres for enough objects to create a statistically robust sample set. Since the late seventies, many
214 attempts have been made at automating strain or fabric analysis to address this (e.g., Peach and Lisle,
215 1979). Initially, the limiting steps in the automation of these strain analysis techniques was the
216 recognition and fitting of best-fit ellipses to geological strain markers, such as sedimentary clasts (Fig.
217 6a & b).

218 The efficient and accurate automatic segmentation of thin section images is still a developing field and
219 has received a lot of recent attention with numerous attempts at automated extraction using image
220 processing or GIS-based techniques (e.g., Goodchild and Fueten, 1998; Heilbronner, 2000; van den
221 Berg et al., 2002; Perring et al., 2004; Barraud, 2006; Choudhury et al., 2006; Li et al., 2008; Tarquini
222 and Favalli, 2010; DeVasto et al., 2012; Gorsevski et al., 2012; Heilbronner and Barrett 2013;

223 Mingireanov Filho et al., 2013; Jungmann et al., 2014; Asmussen et al., 2015). Although these methods
224 produce rapid grain boundary maps, they are typically inaccurate or achieve different results
225 depending on the nature of the image. This is highlighted by the regular use of quartz clasts as strain
226 markers, whereby the automatic identification of their boundaries is complicated by undulose
227 extinction, deformation bands, diffuse boundaries and colour similarities between neighbouring
228 grains. Despite these advances, most methods follow the approach of Mukul (1998), whereby grains
229 used as strain markers are manually traced, and then analysed using image analysis software.

230 A number of methods for automated image analysis have been successfully utilised in the past for
231 geological strain analysis (Ailleres et al., 1995; Erslev and Ge, 1990; Masuda et al., 1991; McNaught,
232 1994; Heilbronner and Barrett, 2013). Panozzo (1984) utilised digitised sets of points representing
233 linear or elliptical objects in her projection method. Mulchrone et al. (2005) developed a parameter
234 extraction program (SAPE) that rapidly extracts the required data by using a simple region-growing
235 algorithm to identify regions of interest. Vollmer developed a similar method, Ellipsefit (Vollmer, 2010,
236 2011, 2017). Many of these techniques are discussed in Heilbronner and Barrett (2013), who have
237 provided a superb overview of image analysis techniques for geological material and it is
238 recommended as a starting point for readers interested in this field.

239 Once grain boundaries have been identified and ellipses are fitted to clasts, the parameters required
240 for a range of strain analysis techniques such as the aspect ratio, orientation, and the centroid of the
241 object can now be easily extracted. For the Rf/Ø method the difficulties in calculating a strain estimate
242 cease once ellipses have been fitted to strain markers; for the centre-to-centre methods the
243 difficulties continue.

244 The accuracy of centre-to-centre strain estimates can be further hampered by the ability to clearly
245 define the vacancy field or central void of the Fry Plot (Fig. 6c), which in a strained sample should
246 represent the strain ellipse (Crespi, 1986; Waldron and Wallace, 2007). A variety of techniques have
247 been applied in order to accurately and objectively define this void (Erslev and Ge, 1990; McNaught,

1994; Waldron and Wallace, 2007; Lisle, 2010; Shan and Xiao, 2011; Reddy and Srivastava, 2012; Mulchrone, 2013). Similar problems exist for defining the curve of the polar plot (Mulchrone, 2013).

In order to reduce the time and labour intensity required, Mulchrone et al. (2013) integrated image analysis, ellipse fitting and parameter extraction, and strain analysis routines for MRL and DTNNM in one workflow. They also included a method for bootstrapping the results in order to produce uncertainty estimates (Fig. 6 e&f). Kumar et al. (2014) carried out a detailed comparison analyses on these methods, and found that the Delaunay Triangulation Method of Mulchrone (2013) and the Continuous Function Method of Waldron and Wallace (2007) were the most accurate. Additionally they concluded that the Delaunay Triangulation Method and the image analysis technique of Reddy and Srivastava (2012) were the most time efficient.

The other method that has stood out is the SURFOR method, first presented by Panozzo (1984, 1987), and discussed in detail in Heilbronner and Barrett (2013). The SURFOR method takes a slightly different approach to fabric or strain analysis compared to the Ramsay family of methods. Rather than focussing on the object orientation or the spatial relationship between objects, the SURFOR method quantifies the fabric based on the shape, size and orientation of 'surfaces' (Heilbronner and Barrett, 2013). The 'surfaces' can be any linear element, such as fractures or grain boundaries. One particular advantage of the SURFOR method over the original Ramsay Rf/Ø method is that it accounts for marker size, with smaller objects having less of an impact on the final strain/anisotropy estimate. A similar approach is taken by Launeau et al. (1990, 1996, 2010), whereby linear filters are used to count intercepts along any arbitrary direction of a digital image. The intercepts technique has shown to be comparable to the MRL and the DTNNM methods in moderate strain regimes, although in low strain regimes there appears to be a discrepancy between the methods (McCarthy et al., 2015). These discrepancies are due to uncertainties in strain estimates in low strain regimes.

Application of strain analysis and advances in strain theory

This contribution has focussed on the significant advances made in geological strain analysis, as outlined above, which have provided a number of valuable insights into geological deformation. Unfortunately, natural deformation is rarely simple or restricted to 2D planes, yet this approach have aided with understanding of complex deformations.

Strain analysis and resulting knowledge of the finite strain state of a point in a rock mass has played a fundamental part in the understanding of the development of tectonic fabrics and foliations (Ramsay and Wood, 1973, Tullis and Wood, 1975). However, nature tends to reveal more by capturing change in strain through time and space, (e.g. porphyroclasts and related structures, layers which are shortened and then stretched, and regions of intense shear where the continuum from low to high strain can be spatially traced). Often the spatial changes can be interpreted as reflecting the temporal deformation history. Ramsay (1967) applied the concept of infinitesimal strain together with that of finite strain to understand deformation history, with the difference between what happens in a short time step compared to that over long time periods helped develop the ideas of progressive strain. This infinitesimal approach was followed by the seminal work of Means et al. (1980) who considered the velocity gradient tensor to conceptualise progressive deformation, and used vorticity to quantify rotational deformation. A detailed discussion of vorticity is beyond the scope of this contribution, and interested readers should consult the work of Fossen and Tikoff (Fossen and Tikoff, 1993; Tikoff and Fossen, 1993; Tikoff and Fossen, 1995; Tikoff and Fossen, 1999; Passchier and Trouw, 2005).

Many of the 2D finite strain methods discussed in previous sections have a natural extension to 3D, but there is still a dearth of 3D strain studies. Methods based on shape (e.g. Shimamoto and Ikeda, 1976; Mulchrone et al., 2003) and inter-object relationships (e.g. Fry, 1979; Mulchrone, 2013) can be readily developed into 3D methods. However, in many cases the primary difficulty rests with acquiring suitable data in 3D in order to apply the methods. Recent technological advances have seen the application of tomography to the acquisition of high quality images of 3D markers in rocks (Louis et al,

297 2006; Adam et al, 2013; Robin and Charles, 2015). This is certain to be an area of future development
298 and will inform finite strain studies and their interpretation in the context of 3D deformation history
299 (Tikoff and Fossen, 1999).

300 Important comparisons have been made between clast-based strain analyses and other methods of
301 quantifying deformation. A number of studies in the seventies and eighties highlighted a close
302 relationship between finite strain estimates and quartz crystallographic fabrics (Marjoribanks, 1976;
303 Miller and Christie, 1981; Lisle, 1985; Law, 1986). Rapid developments in techniques such as Electron
304 Back Scatter Diffraction (EBSD) have largely confirmed this relationship, but also provided insights into
305 deformation at subgrain scales one of the most prominent methods for the determination of preferred
306 orientation of minerals in thin sections (Passchier and Trouw, 2005; Prior et al., 2009).

307 Similar advances in rock deformation studies have been made in the field of Anisotropy of Magnetic
308 Susceptibility (AMS), with Graham (1954) first suggesting that magnetic fabrics could be a valuable
309 tool in petrofabric analysis and establishing a link between layer parallel shortening and AMS. Since
310 this pioneering study there has been a huge volume of work confirming the ability of AMS to
311 determine the orientation-distribution of all minerals and all subfabrics in a specimen, with
312 comprehensive reviews provided by Borradaile and Henry (1997) and Borradaile and Jackson (2010).
313 In direct comparisons of AMS to strain analysis techniques, AMS has been shown to be a highly
314 sensitive and rapid method for quantifying tectonic fabrics (Burmeister et al., 2009; Weil and Yonkee,
315 2009; McCarthy et al., 2015).

316 Other significant contributions of strain analysis includes providing accurate information for structural
317 restorations. Compaction and stratigraphic thickening due to deformation can be estimated and
318 incorporated in the construction of balanced cross sections (Woodward et al., 1986; Protzman and
319 Mitra, 1990; Mitra, 1994). Despite Layer Parallel Shortening (LPS) or internal deformation
320 (compaction, collapse of pore space, dissolution or cleavage formation) being shown to accommodate
321 significant shortening in balanced cross sections from carbonate duplexes (27%; Cooper et al., 1983),

gravity driven thrust systems (18-25%; Butler and Paton, 2010), and analogue models (15-30%; Koyi et al., 2004; Burberry, 2015; Lathrop and Burberry, 2017), strain analysis techniques are rarely applied to balancing cross sections.

Unresolved issues in strain analysis

Hobbs and Talbot (1966) highlighted a few of the limitations of strain analysis a year before Ramsay published his seminal text, and the majority of these seem to prevail today: the initial shapes of many strain markers cannot be measured accurately enough to yield highly accurate estimates; and homogeneous strain is typically assumed. Although these assumptions still prevail, they have largely been accepted to be unresolved. In addition to this, a number of factors add further uncertainty to any strain estimate including: strength and influence of the primary or pre-strain fabric; effects of non-passive strain; and the effects of volume-change, these are discussed below.

Primary fabrics

The largest problem for strain analysis methods is the uncertainty regarding the strength and orientation of an initial primary fabric. Most strain analysis methods, particularly the $R_f/\emptyset$ family of techniques, rely on the assumption that the strain markers have a random initial orientation. Certainly in the case of sedimentary rocks this is rarely true, as most sediments develop a preferred orientation either due to depositional processes or diagenesis (Elliott, 1970; Dunnet and Siddans, 1971; Boulter, 1976; Seymour and Boulter, 1979; De Paor, 1980; Holst, 1982; Paterson and Yu, 1994; Maffione and Morris, 2017).

In a study of undeformed lithologies Holst (1982) found that sections not parallel with bedding had a preferred orientation of clasts along the trace of the bedding plane, while sections parallel to bedding typically had no preferred orientation of clasts. Even if an isotropic or random depositional fabric existed, a preferred orientation typically develops during diagenesis and compaction through active or partly rigid body rotation (Borradaile, 1987). Several efforts have been made to remove the effects

346 of primary fabrics on strain estimates (Elliott, 1970; Dunnet and Siddans, 1971; Matthews et al., 1974;
347 Shimamoto and Ikeda, 1976; Lisle, 1977a; Seymour and Boulter, 1979; Holst, 1982; Wheeler, 1986;
348 DePaor, 1988). Unfortunately, most of these methods utilise one or more of the above assumptions
349 and/or assume the existence of independent information concerning the strain ellipsoid. Some of
350 these assumptions regarding the primary fabrics of sedimentary rocks were highlighted by Patterson
351 and Yu (1994) and include the following: individual grains are spherical prior to straining; orientations
352 and shapes of grain populations define spherical, pre-strain fabric ellipsoids (i.e. grains have an initial
353 uniform distribution); pre-strain fabric ellipsoids are symmetric around bedding; and initial fabrics are
354 recognisable even after straining.

355 Failing to account for any of these factors can lead to considerable errors in strain estimates,
356 particularly in domains with relatively low strains ($R < 1.5$). To account for these errors Patterson and
357 Yu (1994) suggested that a correction should be applied by multiplying the estimated strain ellipsoid
358 by an average pre-strain ellipsoid. Unfortunately, information regarding the magnitude and
359 orientation of the pre-strain ellipsoid is rarely available. Paterson and Yu (1994) compiled XYZ averages
360 for a range of rock types, but this is a limited data set and should be expanded. Regarding the
361 orientation, the estimated strain ellipsoid can be multiplied by the reciprocal pre-strain ellipsoid
362 multiple times in numerous orientations to create an error bracket. Ramsay (1967) showed that all
363 possible combinations of two ellipsoids result in an approximate triangular region on a Flinn plot.
364 Following the methodology of Paterson and Yu (1994), this triangular region is then representative of
365 the error bars of the strain estimate.

366

367 *Non-passive deformation*

368 A key assumption of most current strain analysis techniques is that strain is homogenous and that
369 markers behave in a wholly passive manner in relation to their host material. This breaks down in most
370 natural materials especially when sedimentary clasts are used for strain analysis.

Clearly, the most ideal strain markers are those that were originally spherical, which were then deformed passively with no competency contrast between the marker and the host rock. If this holds true then the final shape of the marker will reflect that of the finite strain ellipsoid (Ramsay, 1967). The fundamental assumption of most strain analysis methods is that there is no competency or ductility contrast between the markers and their matrix/host rock, so that the marker and surrounding rock matrix responded to deformation identically. Unfortunately, clasts and their surrounding matrix rarely deform in a passive manner, due to competency or ductility contrasts between the marker and the host rock. This competency contrast is inherently linked to the viscosity contrast between different clast types and the matrix (Ramsay, 1967; Gay, 1968a,b, 1969; Lisle, 1985b; Freeman, 1987; Freeman and Lisle, 1987; Treagus, 2002; Mulchrone and Walsh, 2006; Czeck et al., 2009). Gay (1968a) pointed out that clasts with a low viscosity deform faster than the bulk rock strain ellipse, while clasts with high viscosities resisted deformation and deformed slower than the bulk rock strain ellipse. Gay (1968a) also noted that the viscosity ratio between a clast and the matrix is dependent on the relative proportion of clasts and matrix. Freeman and Lisle (1987) confirmed that the errors in strain estimates are higher when the clasts represent a small fraction of the bulk rock. This is driven by the high ductility contrast, whereby the majority of strain is accommodated by the weaker matrix. As the clast-to-matrix ratio increases the ductility contrast reduces, potentially caused by the reduced ability of the matrix to flow due to the increase in clast on clast interaction. This separation of strain behaviour between the matrix and clasts is typically termed strain partitioning. This type of behaviour is largely controlled by object concentration and the degree of packing and clast interaction, due to the effect these have on the viscosity contrasts (Gay, 1968a; Lisle et al., 1983; Mandal et al., 2003; Vitale and Mazzoli, 2005). Generally, lithologies with higher object concentrations display reduced effects of strain partitioning, leading to more accurate strain estimates (Mandal et al., 2003; Vitale and Mazzoli, 2005).

While reviewing problems arising from these competency contrasts, Treagus and Treagus (2002) concluded that conglomerates as a whole deformed at an approximately constant viscosity in a linearly viscous manner, but also found that Rf/Ø style methods characterised clast strain whereas the

centre-to-centre methods were more effective at characterising bulk rock strain. This is in part due to two factors: clasts typically only represent 50-70% of the bulk rock (Leeder, 1982); and the Rf/Ø methods only consider clast shape and orientation, while centre-to-centre techniques account for distances between the clasts.

This non-passive deformation can be accounted for by utilising centre-to-centre methods, which include spatial information in the estimates of strain, and provide bulk-rock strain estimates that are closer to true strain values. This has been illustrated in a range of natural settings (Meere et al., 2008, Soares and Dias, 2015). Meere et al. (2008) attributed non-passive deformation to the presence of a relatively incompetent clay-rich matrix, which effectively cushioned clasts from internal deformation. This type of behaviour allows for high degrees of competent clast long-axis alignment achieved by a combination of rigid body rotation, layer boundary slip and particle–particle interactions, with minimal evidence of penetrative deformation, despite evidence from traditional strain markers such as reduction spots and deformed burrows (Meere et al., 2008). In these situations, using the Rf/Ø methods leads to a significant underestimate of strain. More recently, Meere et al. (2016) highlighted the importance of identifying passive clast behaviour and the potential for deformation prior to lithification in understanding the deformation history of a region.

Volume change

Most studies applying the strain analysis techniques discussed, do not account for any potential volume change of the markers. Although Ramsay (1967) had already presented a modified Flinn diagram, which was capable of including some aspect of volume loss, this aspect of strain analysis is typically ignored. Clearly natural deformation rarely occurs in a closed system, and many attempts have been made at estimating volume reduction during deformation, as opposed to diagenetic volume loss. For example, there has been considerable debate regarding the amount of volume loss in slate belts. Sorby (1856) initially suggested that a 50% volume reduction could occur in slates, but settled on ~11% (1908). Wright and Platt (1982) suggested a volume loss of 50% in the Martinsburg Shale of West Virginia. Similar volume reductions were suggested in the Taconic Slate Belt (Goldstein et al., 1995, 1998). Onasch (1994) suggested a range of volume loss of 14-35% in deformed quartz arenites. Similarly, Markley and Wojtal (1996) suggested 10-15% volume loss in an Appalachian mixed siliciclastic sequence. Mosher (1987) analysed the variation in sizes of cobbles in the Purgatory Conglomerate, Rhode Island, and suggested that there could be a volume loss of 23-55% of the original cobble volumes in the areas of most intense deformation.

Despite these reports of significant volume reduction, these large volumes are rarely confirmed by geochemical analyses (Wintsch et al., 1991; Erslev and Ward, 1994; Tan et al., 1995). Similarly, Ramsay and Wood (1973) considered that a 10-20% volume reduction could occur based on density differences between lithified mudstones and slates, and argued that greater volume losses were likely to only occur in the deformation of incompletely consolidated sediments. As discussed earlier shortening values of this magnitude have been identified by in a range of settings (e.g., Cooper et al., 1983; Butler and Paton, 2010; Lathrop & Burberry, 2017).

While volume change has been mathematically incorporated into strain analysis (Gratier, 1983; Onasch and Davis, 1988; Baird and Hudleston, 2007), most rocks lack the necessary strain markers for this type of analysis. Some success has been made using isocon diagrams (Grant, 1986), but these are

typically restricted to discrete shear zones (Srivastava et al., 1995; Bhattacharyya and Hudleston, 2001; Baird and Hudleston, 2007). Other successes in identifying volume loss has come from gravity driven fold and thrust belts, where the amount of extension high on the slope can be compared to the amount of compression towards the toe of the slope (Butler and Paton, 2010).

Conclusions

Determining finite strain has seen significant developments since the seminal contribution of John Ramsay. Through advances in imaging and software, it is easier than ever before to collect large data sets and apply multiple strain analysis techniques rapidly, and there are a number of methods which can incorporate statistical handling of the results. Strain analysis is regularly incorporated into structural studies employing anisotropy of magnetic susceptibility, electron backscatter diffraction, x-ray tomography, microstructural analysis etc., which have not only led to advances in our knowedge of rock deformation processes, but also regional scale understanding. It should be obvious that detailed strain analysis studies are required to understand the spatial variations of strain in deformed terranes, but also the significance of those variations.

Of the many advances outlined here, most of them have been driven by developments in computing, automation and statistical methods, whilst the basis for these strain analysis techniques have by in large remained the same, which is a testament to the initial contribution of Ramsay. We anticipate that the next significant advances in this field will again be largely technologically driven. In particular, 3D imaging of strain markers and 3D strain analysis should become more widespread, and perhaps developed into 4D. Although, there have been advances in applying micro-tomography to geological materials, these techniques are yet to be applied to strain analysis. There is also scope for advances to be made in the extraction of high quality data from images with minimum human intervention e.g., grain boundary identification, and machine learning techniques could be applied to this. The natural optical heterogeneity of geological materials, even in single mineral phases such as quartz due to impurities, inclusions and microstructural features, will always makes the automation of grain

identification challenging. Increasingly the use of non-destructive chemical mapping techniques, for example using electron microscope energy-dispersive X-Ray spectroscopy (QEMSCAN) or Raman spectroscopy, produces outputs that allow the user to filter this heterogeneity thereby making the process of grain boundary identification more manageable. This, coupled with new machine learning techniques, will likely develop into a fully automated process for data acquisition, with strain analysis studies becoming fully automated and significantly more efficient.

Regardless of any future developments, it should be clear that the strain analysis techniques of Ramsay and their modernised equivalents should have a place in every structural geologist's toolbox.

Acknowledgements

We are grateful to Frederick Vollmer and Richard Lisle who both contributed critical and invaluable reviews that enhanced the text. Clare Bond is thanked for patient and helpful editorial assistance. Rachael Ellen is thanked for discussions that improved an earlier version of the manuscript. This paper is published with the permission of the Executive Director of the British Geological Survey (UKRI).

References

Adam, J., Klinkmuiller, M., Schreurs, G., Wienke, B. 2013. Quantitative 3D strain analysis in analogue experiments simulating tectonic deformation: Integration of X-ray computed tomography and digital volume correlation techniques. Journal of Structural Geology, 55, 127-149.

Ailleres, L., Champenois, M., Macaudiere, J., Bertrand, J.., 1995. Use of image analysis in the measurement of finite strain by the normalized Fry method: geological implications for the 'Zone Houillere' (Brianconnais zone, French Alps). Mineralogical Magazine 59, 179–187

Asmussen, P., Conrad, O., Günther, A., Kirsch, M. and Riller, U., 2015. Semi-automatic segmentation of petrographic thin section images using a “seeded-region growing algorithm” with an application to characterize weathered subarkose sandstone. Computers & Geosciences, 83, pp.89-99.

Baird, G.B. and Hudleston, P.J., 2007. Modeling the influence of tectonic extrusion and volume loss on the geometry, displacement, vorticity, and strain compatibility of ductile shear zones. Journal of Structural Geology, 29(10), pp.1665-1678.

Barraud, J., 2006. The use of watershed segmentation and GIS software for textural analysis of thin sections. Journal of Volcanology and Geothermal Research, 154(1-2), pp.17-33.

Bhattacharyya, P. and Hudleston, P., 2001. Strain in ductile shear zones in the Caledonides of northern Sweden: a three-dimensional puzzle. Journal of Structural Geology, 23(10), pp.1549-1565.

494 Borradaile, G.J., 1976. A strain study of a granite–granite gneiss transition and accompanying
495 schistosity formation in the Betic orogenic zone, SE. Spain. Journal of the Geological Society, 132(4),
496 pp.417-428.

497 Borradaile, G., 1987. Anisotropy of magnetic susceptibility: rock composition versus strain.
498 Tectonophysics, 138(2-4), pp.327-329.

499 Borradaile, G.J. and Henry, B., 1997. Tectonic applications of magnetic susceptibility and its anisotropy.
500 Earth-Science Reviews, 42(1-2), pp.49-93.

501 Borradaile, G.J. and Jackson, M., 2004. Anisotropy of magnetic susceptibility (AMS): magnetic
502 petrofabrics of deformed rocks. Geological Society, London, Special Publications, 238(1), pp.299-360.

503 Boulter, C.A., 1976. Sedimentary fabrics and their relation to strain-analysis methods. Geology, 4(3),
504 pp.141-146.

505 Brandon, M.T., 1995. Analysis of geologic strain data in strain-magnitude space. Journal of Structural
506 Geology, 17(10), pp.1375-1385.

507 Breddin, H., 1954. Die tektonische Deformation der Fossilien im Rheinischen Schiefergebirge.
508 Zeitschrift der Deutschen Geologischen Gesellschaft, pp.227-305.

509 Breddin, H., 1957. Tektonische Fossil-und Gesteinsdeformation im Gebiet von St. Goarshausen
510 (Rheinisches Schiefergebirge): Decheniana, 110, pp.289-350.

511 Burberry, C.M., 2015. Spatial and temporal variation in penetrative strain during compression: Insights
512 from analog models. Lithosphere, 7(6), pp.611-624.

513 Burmeister, K.C., Harrison, M.J., Marshak, S., Ferré, E.C., Bannister, R.A. and Kodama, K.P., 2009.
514 Comparison of Fry strain ellipse and AMS ellipsoid trends to tectonic fabric trends in very low-strain
515 sandstone of the Appalachian fold–thrust belt. Journal of Structural Geology, 31(9), pp.1028-1038.

516 Butler, R.W.H. and Paton, D.A., 2010. Evaluating lateral compaction in deepwater fold and thrust belts:
517 How much are we missing from “nature’s sandbox”. GSA Today, 20(3), pp.4-10.

518 Cooper, M.A., Garton, M.R. and Hossack, J.R., 1983. The origin of the Basse Normandie duplex,
519 Boulonnais, France. Journal of Structural Geology, 5(2), pp.139-152.

520 Cloos, E., 1947. Oölite deformation in the South Mountain fold, Maryland. Geol. Soc. Am. Bull. 58,
521 843–918.

522 Choudhury, K.R., Meere, P.A. and Mulchrone, K.F., 2006. Automated grain boundary detection by
523 CASRG. Journal of Structural Geology, 28(3), pp.363-375.

524 Crespi, J.M., 1986. Some guidelines for the practical application of Fry's method of strain analysis.
525 Journal of Structural Geology, 8(7), pp.799-808.

526 Czeck, D.M., Fissler, D.A., Horsman, E. and Tikoff, B., 2009. Strain analysis and rheology contrasts in
527 polymictic conglomerates: an example from the Seine metaconglomerates, Superior Province,
528 Canada. Journal of Structural Geology, 31(11), pp.1365-1376.

529 De Paor, D.G., 1980. Some limitations of the Rf/ϕ technique of strain analysis. Tectonophysics, 64(1-
530 2), pp.T29-T31.

531 De Paor, D.G., 1988. Rf/øf strain analysis using an orientation net. Journal of Structural Geology, 10(4),
532 pp.323-333.

533 De Paor, D.G., 1990. Determination of the strain ellipsoid from sectional data. Journal of Structural
534 Geology, 12(1), pp.131-137.

535 DeSitter, L., 1964. Structural Geology. Mc Graw-Hill.

536 DeVasto, Michael A., Dyanna M. Czeck, and Prajukti Bhattacharyya. "Using image analysis and ArcGIS®
537 to improve automatic grain boundary detection and quantify geological images." Computers &
538 geosciences 49 (2012): 38-45.

539 Dunne, W.M., Onasch, C.M. and Williams, R.T., 1990. The problem of strain-marker centers and the
540 Fry method. Journal of Structural Geology, 12(7), pp.933-938.

541 Dunnet, D., 1969. A technique of finite strain analysis using elliptical particles. Tectonophysics 7, 117–
542 136.

543 Dunnet, D., Siddans, A., 1971. Non-random sedimentary fabrics and their modification by strain.
544 Tectonophysics 12, 307–325.

545 Elliott, D., 1970. Determination of finite strain and initial shape from deformed elliptical objects.
546 Geological Society of America Bulletin 81, 2221–2236.

547 Erslev, E., 1988. Normalized center-to-center strain analysis of packed aggregates. Journal of
548 Structural Geology 10, 201–209.

549 Erslev, E., Ge, H., 1990. Least-squares center-to-center and mean object ellipse fabric analysis. Journal
550 of Structural Geology 12, 1047–1059.

551 Erslev, E. A., & Ward, D. J. (1994). Non-volatile element and volume flux in coalesced slaty cleavage.
552 Journal of Structural Geology, 16(4), 531-553.

553 Flinn, D., 1956. On the deformation of the Funzie conglomerate, Fetlar, Shetland. J. Geol. 480–505.

554 Flinn, D., 1962a. On folding during three-dimensional progressive deformation. Q. J. Geol. Soc. 118.

555 Flinn, D., 1965. On the Symmetry Principle and the Deformation Ellipsoid. Geol. Mag. 102, 36–45.

556 Fossen, H., Tikoff, B. 1993. The deformation matrix for simultaneous simple shearing, pure shearing
557 and volume change, and its applications to transpression-transtension tectonics. Journal of Structural
558 Geology, 15, 413-422.

559 Freeman, B., 1987. The behaviour of deformable ellipsoidal particles in three-dimensional slow flows:
560 implications for geological strain analysis. Tectonophysics, 132(4), pp.297-309.

561 Freeman, B. and Lisle, R.J., 1987. The relationship between tectonic strain and the three-dimensional
562 shape fabrics of pebbles in deformed conglomerates. Journal of the Geological Society, 144(4), pp.635-
563 639.

564 Fry, N., 1979. Random point distributions and strain measurement in rocks. Tectonophysics 60, 89–
565 105.

566 Gay, N.C. 1968a Pure shear and simple shear deformation of inhomogenous viscous fluids. 1. Theory.
567 Tectonophysics 5, p 211-234.

568 Gay, N.C. 1968b Pure shear and simple shear deformation of inhomogenous viscous fluids. 2. The
569 determination of total finite strain in a rock from objects such as deformed pebbles. Tectonophysics
570 5, p 295-302.

571 Gay, N. C. 1969 The analysis of strain in the Barberton Mountain Land, Eastern Transvaal, using
572 deformed pebbles. Journal of Geology 77, p 377-396.

573 Gendzwill, D.J. and Stauffer, M.R., 1981. Analysis of triaxial ellipsoids: Their shapes, plane sections,
574 and plane projections. Journal of the International Association for Mathematical Geology, 13(2),
575 pp.135-152.

576 Goldstein, A., Pickens, J., Klepeis, K. and Linn, F., 1995. Finite strain heterogeneity and volume loss in
577 slates of the Taconic Allochthon, Vermont, USA. Journal of Structural Geology, 17(9), pp.1207-1216.

578 Goldstein, A., Knight, J. and Kimball, K., 1998. Deformed graptolites, finite strain and volume loss
579 during cleavage formation in rocks of the taconic slate belt, New York and Vermont, USA. Journal of
580 structural geology, 20(12), pp.1769-1782.

581 Goodchild, J.S. and Fueten, F., 1998. Edge detection in petrographic images using the rotating polarizer
582 stage. Computers & Geosciences, 24(8), pp.745-751.

583 Gorsevski, P.V., Onasch, C.M., Farver, J.R. and Ye, X., 2012. Detecting grain boundaries in deformed
584 rocks using a cellular automata approach. Computers & Geosciences, 42, pp.136-142.

585 Grant, J.A., 1986. The isocon diagram; a simple solution to Gresens' equation for metasomatic
586 alteration. Economic geology, 81(8), pp.1976-1982.

587 Gratier, J.P., 1983. Estimation of volume changes by comparative chemical analyses in
588 heterogeneously deformed rocks (folds with mass transfer). In Strain Patterns in Rocks (pp. 329-339).

589 Hanna, S., Fry, N., 1979. A comparison of methods of strain determination in rocks from southwest
590 Dyfed (Pembrokeshire) and adjacent areas. Journal of Structural Geology 1, 155–162.

591 Haughton, S., 1856. LII. On slaty cleavage, and the distortion of fossils. London, Edinburgh, Dublin
592 Philos. Mag. J. Sci. 12, 409–421.

593 Heilbronner, R., 2000. Automatic grain boundary detection and grain size analysis using polarization
594 micrographs or orientation images. Journal of Structural Geology 22, 969–981.

595 Heilbronner, R. and Barrett, S., 2013. Image analysis in earth sciences: microstructures and textures
596 of earth materials (Vol. 129). Springer Science & Business Media.

597 Hobbs, B.E. and Talbot, J.L., 1966. The analysis of strain in deformed rocks. The Journal of Geology,
598 74(4), pp.500-513.

599 Hobbs, B.E., Means, W.D. and Williams, P.F., 1976. An outline of structural geology. Wiley.

600 Holst, T.B., 1982. The role of initial fabric on strain determination from deformed ellipsoidal objects.
601 Tectonophysics, 82(3-4), pp.329

602 Hossack, J.R., 1968. Pebble deformation and thrusting in the Bygdin area (southern Norway).
603 Tectonophysics, 5(4), pp.315-339.-350.

604 Hsu, T.C., 1966. The characteristics of coaxial and non-coaxial strain paths. Journal of Strain Analysis,
605 1(3), pp.216-222.

606 Jungmann, M., Pape, H., Wißkirchen, P., Clauser, C. and Berlage, T., 2014. Segmentation of thin section
607 images for grain size analysis using region competition and edge-weighted region merging. Computers
608 & Geosciences, 72, pp.33-48.

609 Koyi, H.A., Sans, M., Teixell, A., Cotton, J. and Zeyen, H., 2004. The significance of penetrative strain in
610 the restoration of shortened layers—Insights from sand models and the Spanish Pyrenees. In K. R.
611 McClay, ed., Thrust tectonics and hydrocarbon systems: AAPG Memoir 82, p. 1–16.

612 Kumar, R., Srivastava, D.C. and Ojha, A.K., 2014. A comparison of the methods for objective strain
613 estimation from the Fry plots. Journal of Structural Geology, 63, pp.76-90.

614 Lathrop, B.A. and Burberry, C.M., 2017. Accommodation of penetrative strain during deformation
615 above a ductile décollement. Lithosphere, 9(1), pp.46-57.

616 Launeau, P., Bouchez, J.L. and Benn, K., 1990. Shape preferred orientation of object populations:
617 automatic analysis of digitized images. Tectonophysics, 180(2-4), pp.201-211.

618 Launeau, P.A., and Robin, P.Y., 1996. Fabric analysis using the intercept method. Tectonophysics,
619 267(1-4), pp.91-119.

620 Launeau, P. and Robin, P.Y.F., 2005. Determination of fabric and strain ellipsoids from measured
621 sectional ellipses—Implementation and applications. Journal of Structural Geology, 27(12), pp.2223-
622 2233.

623 Launeau, P., Archanjo, C.J., Picard, D., Arbaret, L. and Robin, P.Y., 2010. Two-and three-dimensional
624 shape fabric analysis by the intercept method in grey levels. Tectonophysics, 492(1-4), pp.230-239.

625 Law, R.D., 1986. Relationships between strain and quartz crystallographic fabrics in the Roche Maurice
626 quartzites of Plougastel, western Brittany. Journal of Structural Geology, 8(5), pp.493-515.

627 Leeder, M.R., 1982. Sedimentology: process and product. Springer.

628 Li, Y., Onasch, C.M. and Guo, Y., 2008. GIS-based detection of grain boundaries. Journal of Structural
629 Geology, 30(4), pp.431-443.

630 Lisle, R., 1977a. Estimation of the tectonic strain ratio from the mean shape of deformed elliptical
631 objects. Geologie en Mijnbouw 56, 140–144.

632 Lisle, R., 1977b. Clastic grain shape and orientation in relation to cleavage from the Aberystwyth Grits,
633 Wales. Tectonophysics 39, 381–395.

634 Lisle, R.J., Rondeel, H.E., Doorn, D., Brugge, J. and Van de Gaag, P., 1983. Estimation of viscosity
635 contrast and finite strain from deformed elliptical inclusions. Journal of Structural Geology, 5(6),
636 pp.603-609.

637 Lisle, R., 1985. Geological Strain Analysis: A Manual for the Rf/φ Method. Pergamon Press.

638 Lisle, R.J., 1985b. The effect of composition and strain on quartz-fabric intensity in pebbles from a
639 deformed conglomerate. Geologische Rundschau, 74(3), pp.657-663.

640 Lisle,R., 1994. Palaeostrain Analysis. In P.L. Hancock (Ed.), Continental Deformation, Pergamon Press,
641 pp. 28-42.

642 Lisle, R.J., 2010. Strain analysis from point fabric patterns: An objective variant of the Fry method.
643 Journal of Structural Geology, 32(7), pp.975-981.

644 Louis, L., Wong, T., Buad, P. Tembe, S. 2006. Imaging strain localization by X-ray computed
645 tomography: discrete compaction bands in Diemelstadt sandstone. Journal of Structural Geology, 28,
646 762-775.

647 Maffione, M. and Morris, A., 2017. The onset of fabric development in deep marine sediments. Earth
648 and Planetary Science Letters, 474, pp.32-39.

649 Mandal, N., Samanta, S.K., Bhattacharyya, G. and Chakraborty, C., 2003. Deformation of ductile
650 inclusions in a multiple inclusion system in pure shear. Journal of Structural Geology, 25(9), pp.1359-
651 1370.

652 Marjoribanks, R.W., 1976. The relation between microfabric and strain in a progressively deformed
653 quartzite sequence from central Australia. Tectonophysics, 32(3-4), pp.269-293.

654 Markley, M. and Wojtal, S., 1996. Mesoscopic structure, strain, and volume loss in folded cover strata,
655 Valley and Ridge Province, Maryland. American Journal of Science, 296(1), pp.23-57.

656 Masuda, T., Koike, T., Yuko, T. and Morikawa, T., 1991. Discontinuous grain growth of quartz in
657 metacherts: the influence of mica on a microstructural transition. Journal of Metamorphic Geology,
658 9(4), pp.389-402.

659 Matthews, P.E., Bond, R.A.B. and Van Den Berg, J.J., 1974. An algebraic method of strain analysis using
660 elliptical markers. Tectonophysics, 24(1-2), pp.31-67.

661 McCarthy, D.J., Meere, P.A. and Petronis, M.S., 2015. A comparison of the effectiveness of clast based
662 finite strain analysis techniques to AMS in sandstones from the Sevier Thrust Belt, Wyoming.
663 Tectonophysics, 639, pp.68-81.

664 McNaught, M, 1994. Modifying the normalized Fry method for aggregates of non-elliptical grains.
665 Journal of Structural Geology, 16(4), pp.493-503.

666 Means, W.D., Hobbs, B.E., Lister, G.S., Williams, P.F. 1980. Vorticity and non-coxiality in progressive
667 deformation. Journal of Structural Geology, 2, 371-378.

668 Meere, P.A., Mulchrone, K.F., Sears, J.W. and Bradway, M.D., 2008. The effect of non-passive clast
669 behaviour in the estimation of finite strain in sedimentary rocks. Journal of Structural Geology, 30(10),
670 pp.1264-1271.

671 Meere, P.A., Mulchrone, K.F., McCarthy, D.J., Timmerman, M.J. and Dewey, J.F., 2016. Prelithification
672 and synlithification tectonic foliation development in a clastic sedimentary sequence. Geology, 44(4),
673 pp.291-294.

674 Miller, D.M. and Christie, J.M., 1981. Comparison of quartz microfabric with strain in recrystallized
675 quartzite. Journal of Structural Geology, 3(2), pp.129-141.

676 Milton, N.J., 1980. Determination of the strain ellipsoid from measurements on any three sections.
677 Tectonophysics, 64(1-2), pp.T19-T27.

678 Mingireanov Filho, I., Spina, T.V., Falcão, A.X. and Vidal, A.C., 2013. Segmentation of sandstone thin
679 section images with separation of touching grains using optimum path forest operators. Computers &
680 Geosciences, 57, pp.146-157.

681 Mitra, G., 1994. Strain variation in thrust sheets across the Sevier fold-and-thrust belt (Idaho-Utah-
682 Wyoming): Implications for section restoration and wedge taper evolution. Journal of Structural
683 Geology, 16(4), pp.585-602.

684 Mookerjee, M., Nickleach, S., 2011. Three-dimensional strain analysis using Mathematica. J. Struct.
685 Geol. 33, 1467–1476.

686 Mookerjee, M. and Peek, S., 2014. Evaluating the effectiveness of Flinn's k-value versus Lode's ratio.
687 Journal of Structural Geology, 68, pp.33-43.

688 Mosher, S., 1987. Pressure-solution deformation of the Purgatory Conglomerate, Rhode Island (USA):
689 quantification of volume change, real strains and sedimentary shape factor. Journal of structural
690 geology, 9(2), pp.221-232.

691 Mukul, M., 1998. A spatial statistics approach to the quantification of finite strain variation in
692 penetratively deformed thrust sheets: an example from the Sheeprock Thrust Sheet, Sevier. Journal
693 of Structural Geology20, 371–384.

694 Mulchrone, K.F. and Meere, P.A., 2001. A Windows program for the analysis of tectonic strain using
695 deformed elliptical markers. Computers & geosciences, 27(10), pp.1251-1255.

696 Mulchrone, K.F., 2003. Application of Delaunay triangulation to the nearest neighbour method of
697 strain analysis. Journal of Structural Geology, 25(5), pp.689-702.

698 Mulchrone, K.F., O'Sullivan, F. and Meere, P.A., 2003. Finite strain estimation using the mean radial
699 length of elliptical objects with bootstrap confidence intervals. Journal of Structural Geology, 25(4),
700 pp.529-539.

701 Mulchrone, K.F., Meere, P.A. and Choudhury, K.R., 2005. SAPE: a program for semi-automatic
702 parameter extraction for strain analysis. Journal of structural geology, 27(11), pp.2084-2098.

703 Mulchrone, K.F. and Walsh, K., 2006. The motion of a non-rigid ellipse in a general 2D deformation.
704 Journal of Structural Geology, 28(3), pp.392-407.

705 Mulchrone, K.F., 2013. Fitting the void: Data boundaries, point distributions and strain analysis.
706 Journal of Structural Geology, 46, pp.22-33.

707 Mulchrone, K.F., McCarthy, D.J. and Meere, P.A., 2013. Mathematica code for image analysis, semi-
708 automatic parameter extraction and strain analysis. Computers & Geosciences, 61, pp.64-70.

709 Nádai, A., 1950. Theory of flow and fracture of solids, v. 2.

710 Oertel, G., 1978. Strain determination from the measurement of pebble shapes. Tectonophysics,
711 50(1), pp.T1-T7.

712 Onasch, C.M., 1986. Ability of the Fry method to characterize pressure-solution deformation.
713 Tectonophysics, 122(1-2), pp.187-193.

714 Onasch, C.M., 1994. Assessing brittle volume-gain and pressure solution volume-loss processes in
715 quartz arenite. Journal of Structural Geology, 16(4), pp.519-530.

716 Onasch, C.M. and Davis, T.L., 1988. Strain determination using cathodoluminescence of calcite
717 overgrowths. Journal of structural geology, 10(3), pp.301-303.

718 Owens, W.H., 1984. The calculation of a best-fit ellipsoid from elliptical sections on arbitrarily
719 orientated planes. J. Struct. Geol. 6, 571–578.

720 Panozzo, R., 1984. Two-dimensional strain from the orientation of lines in a plane. Journal of Structural
721 Geology 6, 215–221.

722 Panozzo, R., 1987. Two-dimensional strain determination by the inverse SURFOR wheel. Journal of
723 Structural Geology, 9(1), pp.115-119.

724 Park, R.G., 1997. Foundation of structural geology. Routledge.

725 Passchier, C.W. and Trouw, R.A., 2005. Microtectonics (Vol. 1). Springer Science & Business Media.

726 Paterson, S., Yu, H., 1994. Primary fabric ellipsoids in sandstones: implications for depositional
727 processes and strain analysis. J. Struct. Geol. 16, 505–517.

728 Peach, C., and Lisle, R., 1979. A Fortran IV program for the analysis of tectonic strain using deformed
729 elliptical markers. Computers & Geosciences 5, 325–334.

730 Perring, C.S., Barnes, S.J., Verrall, M. and Hill, R.E.T., 2004. Using automated digital image analysis to
731 provide quantitative petrographic data on olivine–phyric basalts. Computers & Geosciences, 30(2),
732 pp.183-195.

733 Phillips, J., 1843. On certain movements in the parts of stratified rocks. Adv. Sci, pp.60-61.

734 Prior, D.J., Mariani, E. and Wheeler, J., 2009. EBSD in the earth sciences: applications, common
735 practice, and challenges. In Electron backscatter diffraction in materials science (pp. 345-360).
736 Springer, Boston, MA.

737 Protzman, G.M. and Mitra, G., 1990. Strain fabric associated with the Meade thrust sheet: implications
738 for cross-section balancing. Journal of Structural Geology, 12(4), pp.403-417.

739 Ramsay, J.G., 1967. Folding and fracturing of rocks. New York, MacGraw-Hill, 568p

740 Ramsay, J.G. and Wood, D.S., 1973. The geometric effects of volume change during deformation
741 processes. Tectonophysics, 16(3-4), pp.263-277.

742 Ramsay, J.G., and Huber, M., 1983. The techniques of modern structural geology. Strain Analysis,
743 London: Academic Press.

744 Reddy, B.S.R. and Srivastava, D.C., 2012. Rapid extraction of central vacancy by image-analysis of Fry
745 plots. Journal of Structural Geology, 40, pp.44-53.

746 Robin, P., 1977. Determination of geologic strain using randomly oriented strain markers of any shape.
747 Tectonophysics 42, T7–T16.

748 Robin, P.-Y.F., 2002. Determination of fabric and strain ellipsoids from measured sectional ellipses —
749 theory. J. Struct. Geol. 24, 531–544.

750 Robin P.F., Charles, C.R.J. 2015. Quantifying the three-dimensional shapes of spheroidal objects in
751 rocks imaged by tomography. Journal of Structural Geology, 77, 1-10.

752 Seymour, D.B. and Boulter, C.A., 1979. Tests of computerised strain analysis methods by the analysis
753 of simulated deformation of natural unstrained sedimentary fabrics. Tectonophysics, 58(3-4), pp.221-
754 235.

755 Shan, Y., 2008. An analytical approach for determining strain ellipsoids from measurements on planar
756 surfaces. Journal of Structural Geology, 30(4), pp.539-546

757 Shan, Y. and Xiao, W., 2011. A statistical examination of the Fry method of strain analysis. Journal of
758 Structural Geology, 33(5), pp.1000-1009.

759 Shao, J. and Wang, C., 1984. Determination of strain ellipsoid according to two-dimensional data on
760 three or more intersection planes. Journal of the International Association for Mathematical Geology,
761 16(8), pp.823-833.

762 Sharpe, D., 1847. On slaty cleavage. Q. J. Geol. Soc. 3, 74–105.

763 Shimamoto, T., Ikeda, Y., 1976. A simple algebraic method for strain estimation from deformed
764 ellipsoidal objects. 1. Basic theory. Tectonophysics 36, 315–337.

765 Siddans, A.W.B., 1980. Analysis of three-dimensional, homogeneous, finite strain using ellipsoidal
766 objects. Tectonophysics, 64(1-2), pp.1-16.

767 Soares, A. and Dias, R., 2015. Fry and Rf/φ strain methods constraints and fold transection
768 mechanisms in the NW Iberian Variscides. Journal of Structural Geology, 79, pp.19-30.

769 Sorby, H., 1849. On the origin of slaty cleavage. Proc. Geol. Polytech. Soc. West Rid. Yorksh. 3, 300–
770 312.

771 Sorby, H., 1856. XVIII. On the theory of the origin of slaty cleavage. London, Edinburgh, Dublin Philos.
772 Mag. J. Sci. 12, 127–129.

773 Sorby, H.C., 1908. On the application of quantitative methods to the study of the structure and history
774 of rocks. Quarterly Journal of the Geological Society, 64(1-4), pp.171-233.

775 Srivastava, H.B., Hudleston, P. and Earley III, D., 1995. Strain and possible volume loss in a high-grade
776 ductile shear zone. Journal of Structural Geology, 17(9), pp.1217-1231.

777 Tan, B.K., Gray, D.R. and Stewart, I., 1995. Volume change accompanying cleavage development in
778 graptolitic shales from Gisborne, Victoria, Australia. Journal of Structural Geology, 17(10), pp.1387-
779 1394.

780 Tarquini, S. and Favalli, M., 2010. A microscopic information system (MIS) for petrographic analysis.
781 Computers & Geosciences, 36(5), pp.665-674.

782 Tikoff, B, Fossen, H. 1993. Simultaneous pure and simple shear: the unifying deformation matrix.
783 Tectonophysics, 217, 267-283.

784 Tikoff, B, Fossen, H. 1995. The limitations of three dimensional kinematic vorticity analysis. Journal of
785 Structural Geology, 17, 1771-1784.

786 Tikoff, B, Fossen, H. 1999. Three dimensional reference deformations and strain facies. Journal of
787 Structural Geology, 21, 1497-1512.Todd, S.P., 2000, Taking the roof off a suture zone: basin setting
788 and provenance of conglomerates in the ORSDingle Basin of SW Ireland: Geological Society, London,
789 Special Publications, v. 180, no. 1, p. 185–222.

790 Treagus, S.H., 2002. Modelling the bulk viscosity of two-phase mixtures in terms of clast shape. Journal
791 of Structural Geology, 24(1), pp.57-76.

792 Treagus, S.H., and Treagus, J.E., 2002. Studies of strain and rheology of conglomerates. J. Struct. Geol.
793 24, 1541–1567.

794 Van den Berg, E.H., Meesters, A.G.C.A., Kenter, J.A.M. and Schlager, W., 2002. Automated separation
795 of touching grains in digital images of thin sections. Computers & Geosciences, 28(2), pp.179-190.

796 Vitale, S. and Mazzoli, S., 2005. Influence of object concentration on finite strain and effective viscosity
797 contrast: insights from naturally deformed packstones. Journal of Structural Geology, 27(12), pp.2135-
798 2149.

799 Vollmer, F. W., 2010. A comparison of ellipse-fitting techniques for two and three-dimensional strain
800 analysis, and their implementation in an integrated computer program designed for field-based
801 studies. Abstract T21B-2166, Fall Meeting, American Geophysical Union, San Francisco, California.

802 Vollmer, F. W., 2011. Best-fit strain from multiple angles of shear and implementation in a computer
803 program for geological strain analysis. Geological Society of America Abstracts with Programs, v. 43.

804 Vollmer, F. W., 2017. EllipseFit: Strain and Fabric Analysis Software User Manual Version 3.4.0
805 [computer software user manual]. Retrieved from http://www.frederickvollmer.com/ellipsefit/.

Waldron, J.W. and Wallace, K.D., 2007. Objective fitting of ellipses in the centre-to-centre (Fry) method of strain analysis. Journal of Structural Geology, 29(9), pp.1430-1444.

Weil, A.B. and Yonkee, A., 2009. Anisotropy of magnetic susceptibility in weakly deformed red beds from the Wyoming salient, Sevier thrust belt: Relations to layer-parallel shortening and orogenic curvature. Lithosphere, 1(4), pp.235-256.

Wheeler, J., 1986. Strain analysis in rocks with pretectonic fabrics. Journal of structural geology, 8(8), pp.887-896.

Wintsch, R.P., Kvale, C.M. and Kisch, H.J., 1991. Open-system, constant-volume development of slaty cleavage, and strain-induced replacement reactions in the Martinsburg Formation, Lehigh Gap, Pennsylvania. Geological Society of America Bulletin, 103(7), pp.916-927.

Woodward, N.B., Gray, D.R. and Spears, D.B., 1986. Including strain data in balanced cross-sections. Journal of Structural Geology, 8(3-4), pp.313-324.

Wright, T.O. and Platt, L.B., 1982. Pressure dissolution and cleavage in the Martinsburg Shale. American Journal of Science, 282(2), pp.122-135.

Yu, H., Zheng, Y., 1984. A statistical analysis applied to the Rf/φ method. Tectonophysics 110, 151–155.

Zingg, T., 1935. Beitrag zur schotteranalyse (Doctoral dissertation, ETH Zurich).

Figure Captions

Fig. 1 Identifying strain in rocks. A. A highly idealised rock outcrop with three exposed mutually perpendicular surfaces, with appropriate strain markers on each surface. The strain ellipsoid illustrates the relationship between the tectonic stretching axes XYZ and sigma 1, 2 & 3. B. A real outcrop from the Dingle Peninsula, which presents a more challenging problem for identifying and quantifying strain.

Fig. 2 A. Measuring the long (M) and short (m) axes of elliptical strain markers. B. Plot of the long and short axes from A. The slope of a best-fit line that passes through the points and the origin provides an estimate of the strain ratio. C. Measuring chords along three defined directions for a population of ellipses.

Fig. 3 Nearest-neighbour and or centre-to-centre methodology. A. Centre to centre techniques are based on the assumption that the tie-lines between nearest neighbours have a uniformly random distribution in the unstrained state. The lengths, d, and orientations, α, of tie lines joining object centres are marked. The Polar plot of the unstrained state is illustrated below, showing d vs α. Interestingly, this unstrained sample has a weak preferred distribution, in that the clasts are closer together in the vertical direction than the horizontal direction. B. Initial strained state, the distances between clasts become shorter in the tectonic shortening direction. The polar plot indicates higher strain estimates. The apex of the curve shows the orientation of the longest direction and the nadir shows the orientation of the shortest direction. C. The final strain state with pressure solution and a higher strain estimate.

Fig. 4 The Rf/Ø method. A. After fitting ellipses to strain markers, the ratio of the long axis to short axis is calculated and the orientation relative to a reference angle is recorded. B. These ratios are then plotted against the orientation of the long axis. This limited data set suggests that preferred orientation is between 45 degrees and 75 degrees. Clearly more data is required to more accurately estimate strain.

Fig. 5. Flinn and Nadai-Hsu plots. A. Flinn plots represent all possible ellipsoid geometries in a 2D space. The standard convention is to use a logarithmic plot, where the ratio of the maximum to intermediate ellipsoid axes (Ln X/Y) is plotted as ordinate and the ratio of the minimum to intermediate axes (Ln Y/Z) is plotted as abscissa. Prolate spheroids plot along the vertical axis and oblate spheroids plot along the horizontal. As these ellipsoids become less spherical, they plot further away from the origin. B. Nadai-Hsu plots show similar information to the Flinn Plots, but have an advantage that less deformed ellipsoids plot closer together regardless of shape.

Fig. 6. Typical strain analysis methodology. A. Selection of a suitable oriented thin section. B. Fitting ellipses to the clasts shown in A. C. Fitting the central void of the Fry Plot. D. The same data is presented in a polar plot. E. Strain estimate from the DTNNM method represented by the black star. The shaded ellipses represent the Bootstrapped confidence intervals. F. Strain estimate from the MRL method represented by the black star. The shaded ellipses represent the Bootstrapped confidence intervals. Note the underestimate compared to the DTNNM method.

Figure

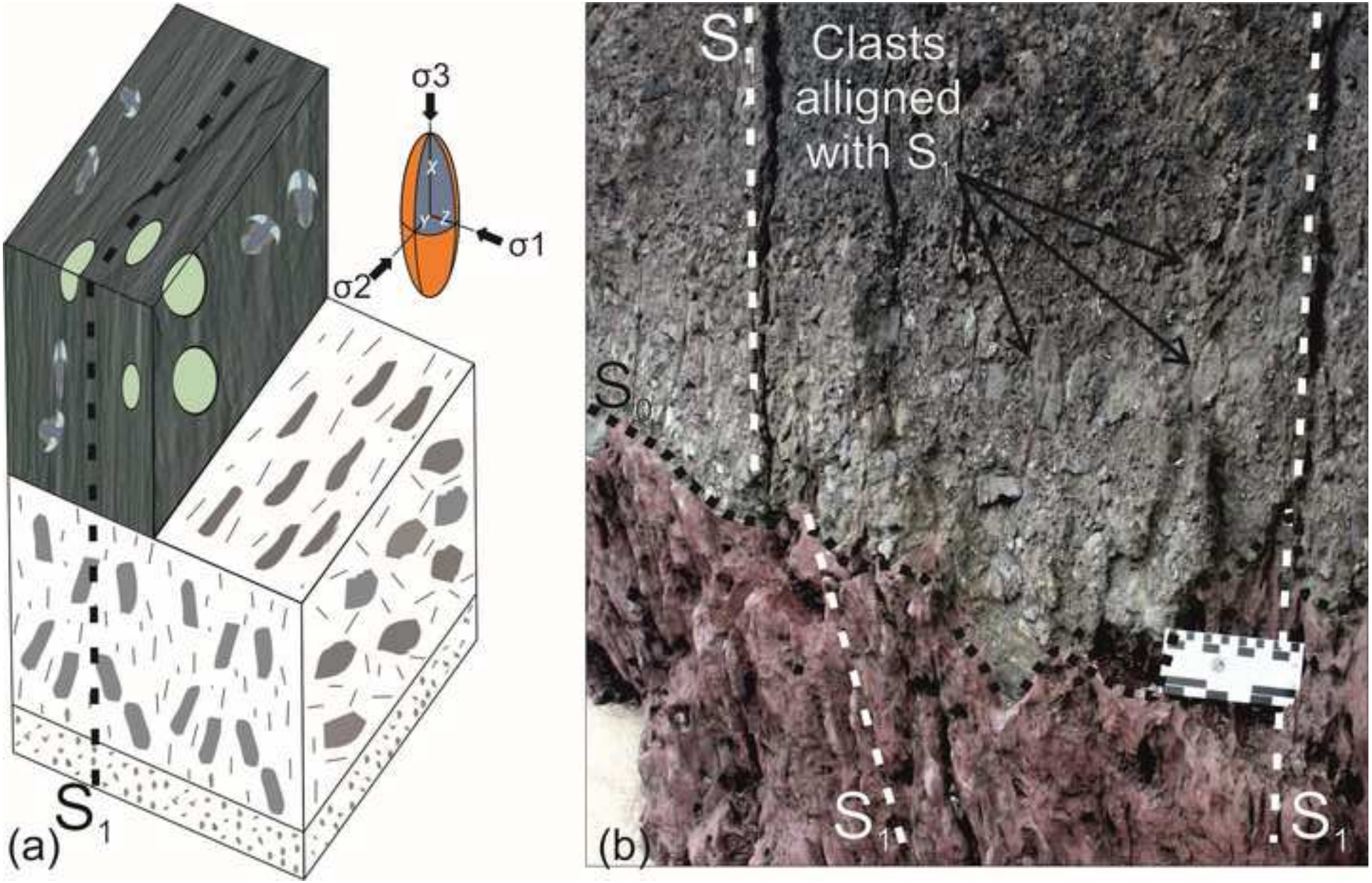

Figure

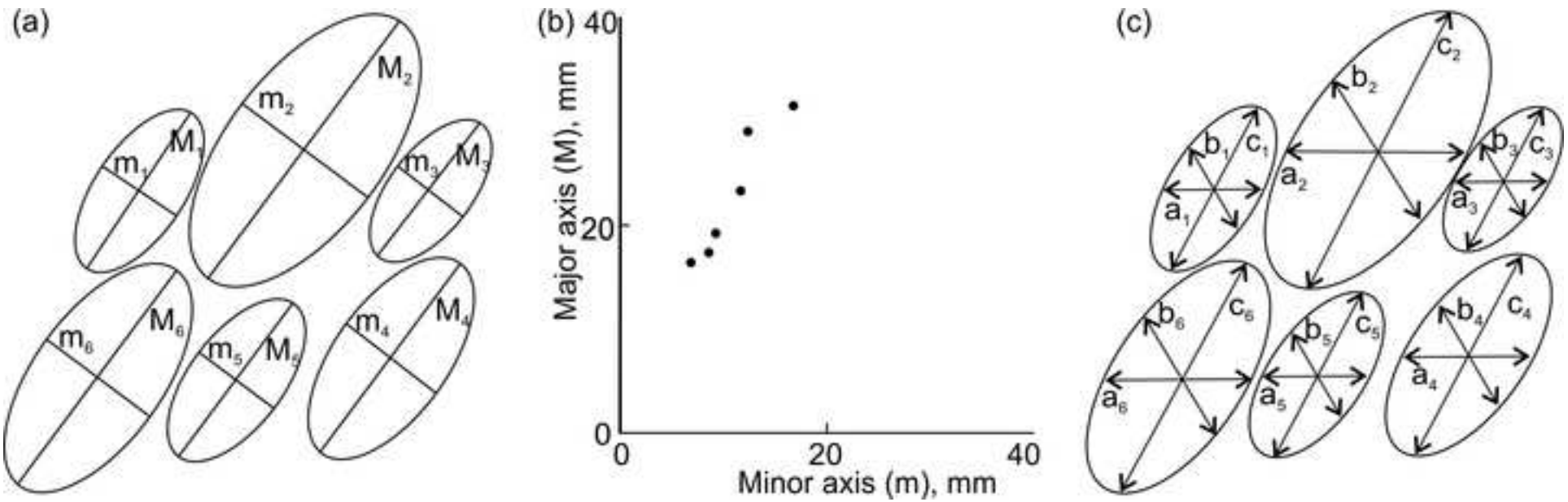
(a)
m1
M1
m2
M2
m3
M3
m4
M4
m5
M5
m6
M6
(b)
Major axis (M), mm
Minor axis (m), mm
0
20
40
0
20
40
(c)
a1
b1
c1
a2
b2
c2
a3
b3
c3
a4
b4
c4
a5
b5
c5
a6
b6
c6

Figure

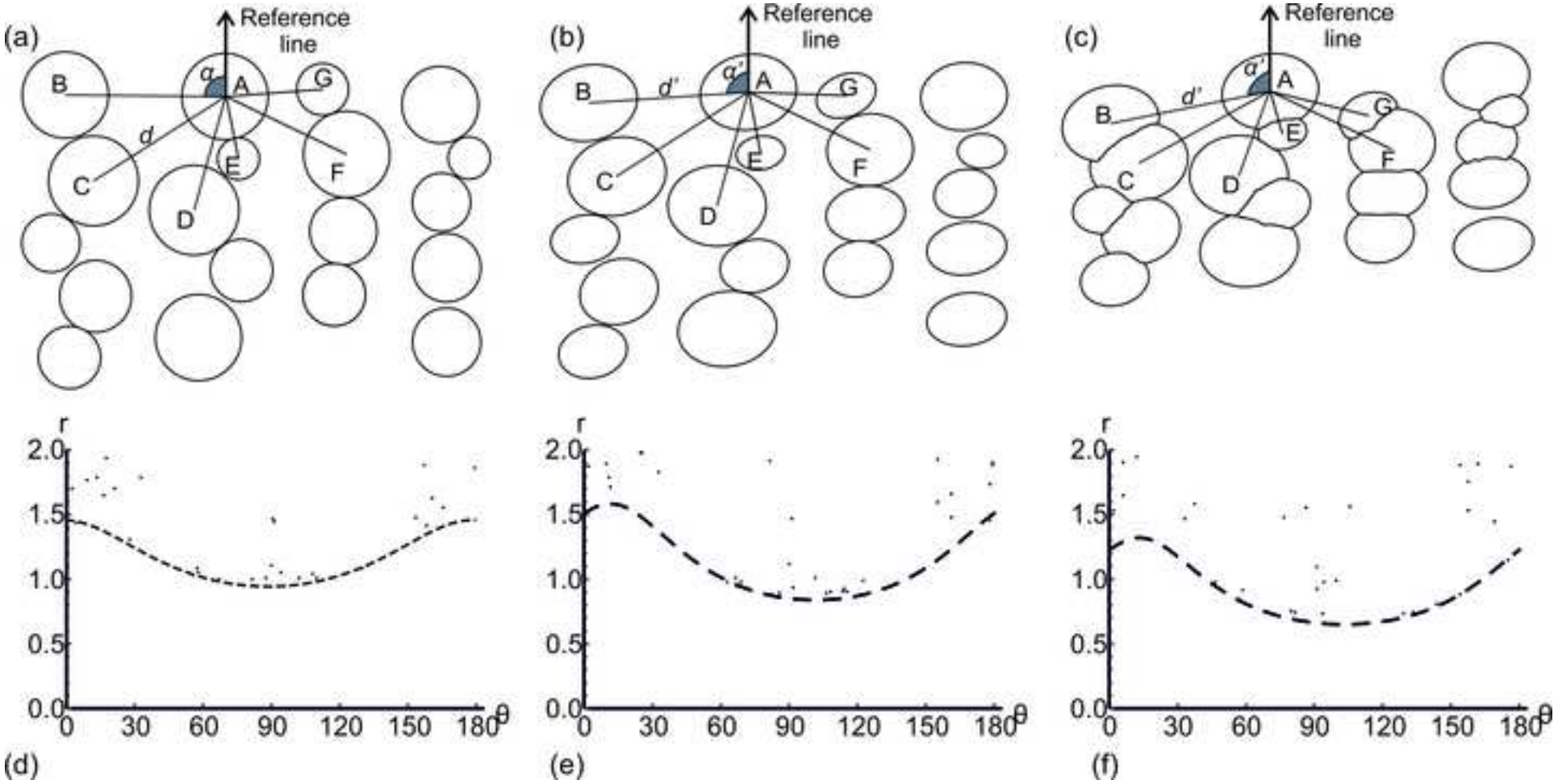
(a)
Reference line
α
A
B
G
d
C
E
F
D
(b)
Reference line
α'
A
B
d'
G
C
E
F
D
(c)
Reference line
α'
A
d'
B
G
E
C
D
F
r
2.0
1.5
1.0
0.5
0.0
0
30
60
90
120
150
180
θ
(d)
(e)
(f)

Figure

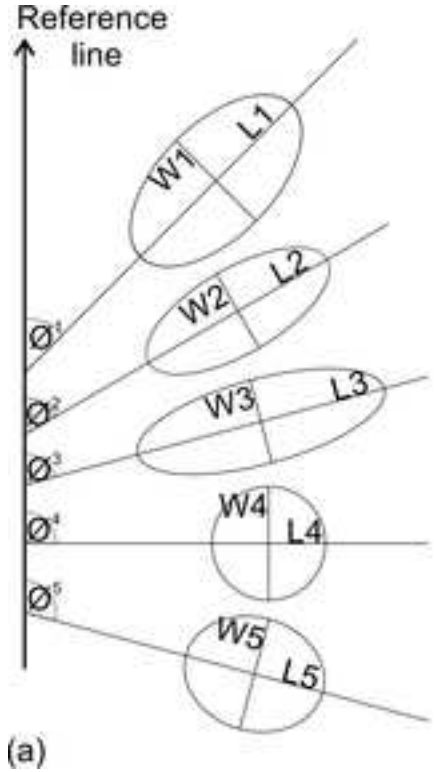
Reference line
W1
L1
W2
L2
W3
L3
W4
L4
W5
L5
Ø1
Ø2
Ø3
Ø4
Ø5

(a)

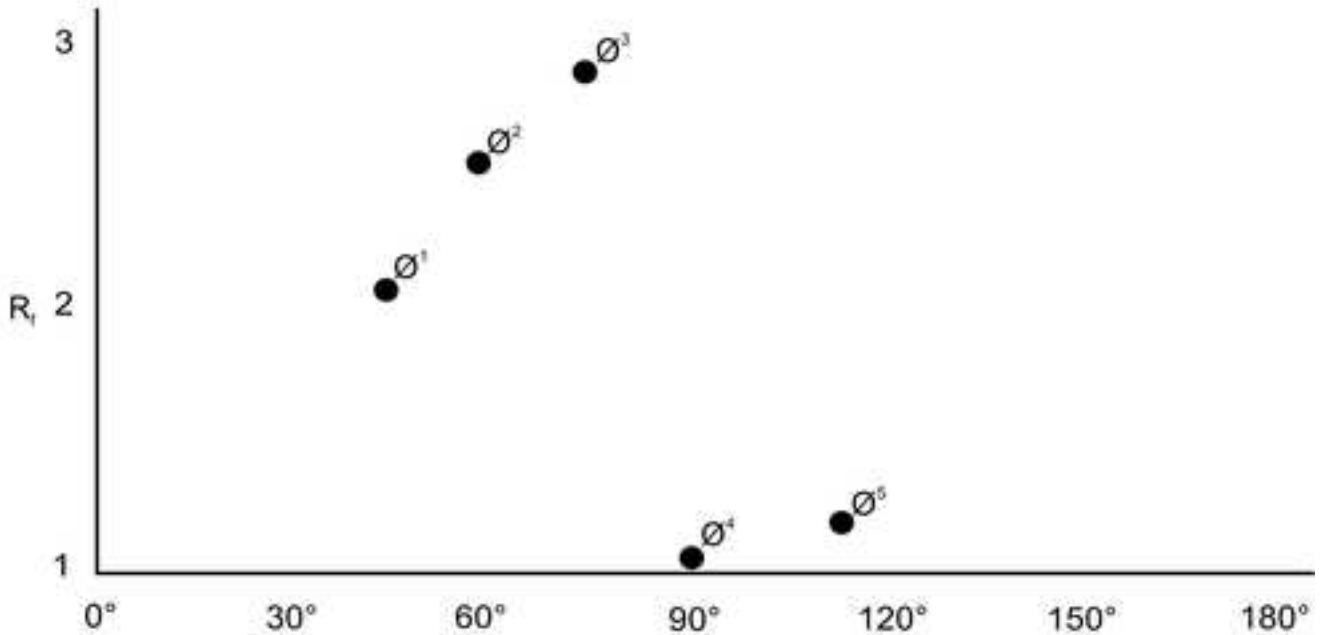
3
2
1
R1
Ø1
Ø2
Ø3
Ø4
Ø5
0°
30°
60°
90°
120°
150°
180°
Angle Ø

(b)

Figure

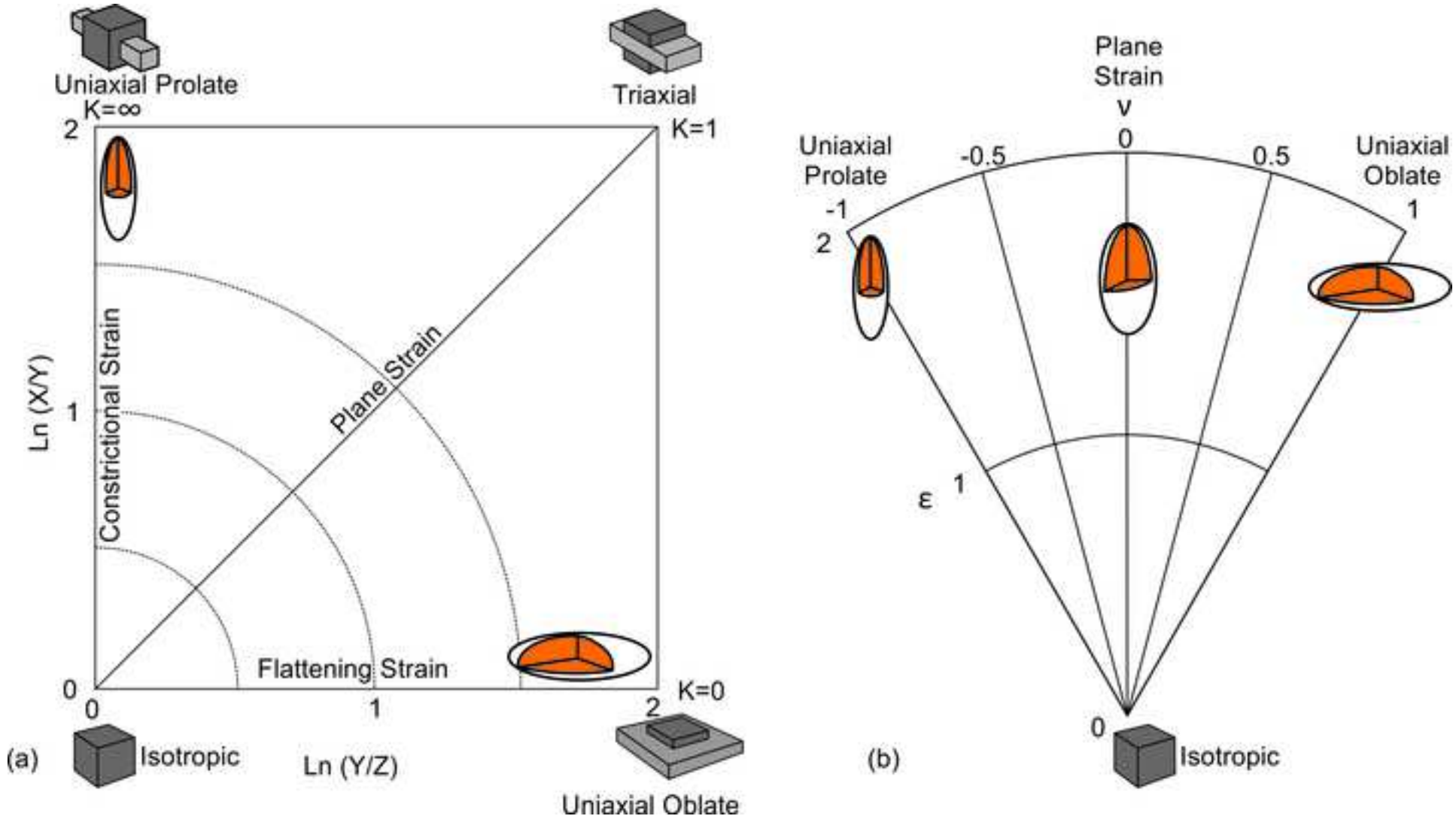
Uniaxial Prolate
K=∞
Triaxial
K=1
2
1
0
Ln (X/Y)
Constrictional Strain
Plane Strain
Flattening Strain
0
1
2
K=0
(a)
Isotropic
Ln (Y/Z)
Uniaxial Oblate
Plane
Strain
ν
0
Uniaxial
Prolate
-0.5
0.5
Uniaxial
Oblate
-1
1
2
ε
1
0
(b)
Isotropic

Figure

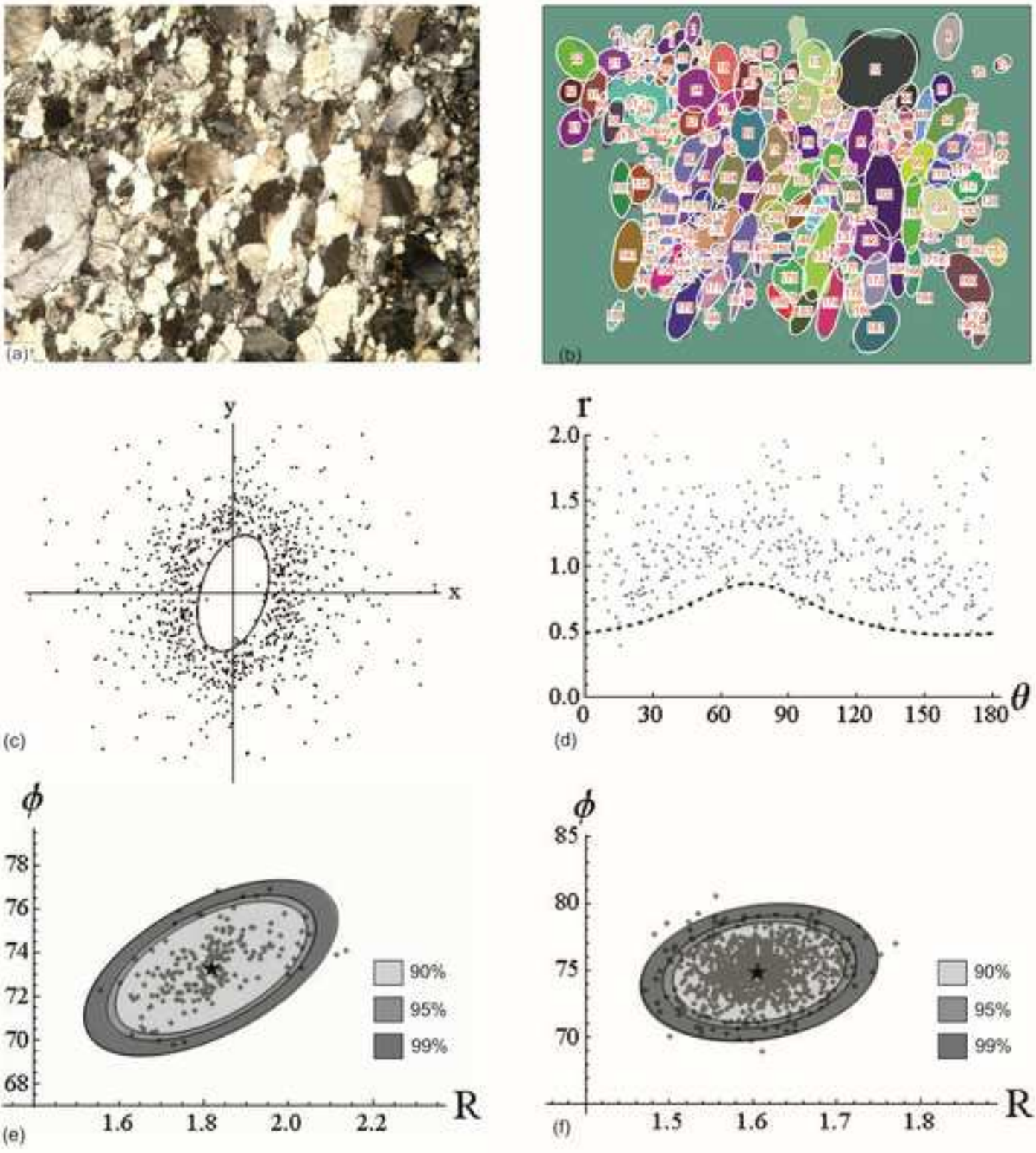
(a)
(b)
y
x
(c)
Γ
2.0
1.5
1.0
0.5
0.0
0
30
60
90
120
150
180
θ
(d)
ϕ
78
76
74
72
70
68
1.6
1.8
2.0
2.2
R
90%
95%
99%
(e)
ϕ
85
80
75
70
1.5
1.6
1.7
1.8
R
90%
95%
99%
(f)